

RESEARCH PAPER

Synthesis and Characterization ZnS-Ni Nanoparticles-Loaded Coconut Shell Activated Carbon for Removal of Crystal Violet: Experimental Design and Optimization

Parisa Rostami ¹, Tahereh Momeni Isfahani ^{2*}, Farnaz Maghazei ³

¹ Master of Science Student in Nano Chemistry, Arak Branch, Islamic Azad University, Arak, Iran

² Department of Chemistry, Faculty of Science, Arak Branch, Islamic Azad University, Arak, Iran

³ Department of mathematics and physics, Faculty of Science, Arak Branch, Islamic Azad University, Arak, Iran

ARTICLE INFO

Article History:

Received 12 February 2022

Accepted 07 June 2022

Published 01 July 2022

Keywords:

Adsorption

Central composite design

Coconut husk activated carbon

Crystal Violet

ZnS-Ni nanoparticles

ABSTRACT

In this work, we used ZnS-Ni/coco AC nanocomposite as a cheap adsorbent for the elimination of Crystal Violet (CV) dye from an aqueous medium by ultrasound based adsorption method. First ZnS-Ni nanoparticles were synthesized by using microwave assisted co-precipitation method. These nanoparticles were then stabilized on activated carbons derived from coconut shells. The ZnS-Ni/coco AC composite was characterized using X-ray diffraction (XRD), field emission scanning electron microscopy (FESEM), transmitted electron microscopy (TEM) and energy-dispersive X-ray spectrometry (EDX). WE used response surface methodology (RSM) based on the central composite design (CCD) to study the effects of four various parameters including dye concentration, the amount of adsorbent, sonication time and pH on the process of adsorption. The optimal condition for removal of CV up to 98.96% was achieved for pH=6.31, 0.023 g of adsorbent for 16.06 mg/L dye concentration and sonication time of 5 minutes. Adsorption equilibrium and kinetic data were fitted with the Langmuir monolayer isotherm model ($q_{\max} = 178.57$ mg/g and $R^2 = 0.9925$) and like pseudo second-order kinetics mechanism ($R^2 = 0.9994$).

How to cite this article

Rostami P, Momeni Isfahani T, Maghazei F. Synthesis and Characterization ZnS-Ni Nanoparticles-Loaded Coconut Shell Activated Carbon for Removal of Crystal Violet: Experimental Design and Optimization. J Nanostruct, 2022; 12(3):529-545.

DOI: 10.22052/JNS.2022.03.006

INTRODUCTION

In today's life, the lack of safe water is one of the main problems of human societies, so there's no wonder that treatment of toxic and nontoxic pollutants from the water resource has become of great importance [1-3]. One of the most well-known toxic pollutants for the environment and water resources are chemical dyes, which are widely present in industries such as textile, tanning,

paper making, pharmaceuticals, plastic, carpet, food and cosmetic industries [4, 5]. The dyes used in these industries are mainly of organic origin and are derived from diazo salts, phthalocyanine and anthraquinone which have benzene rings [6-10]. It is necessary to point out that these dyes are water soluble and have great chemical stability and are highly carcinogenic [11-14].

Crystal Violet or Methyl Violet 10B with chemical

* Corresponding Author Email: t.momeni@iau-arak.ac.ir

formula ($C_{25}H_{30}N_3Cl$) is one of the azo dyes that is widely used in textile, paper and dyeing industries. Crystal Violet (CV) is also used as a preservant factor to prevent the growth of mold, fungi and intestinal parasites in animal feed.

Despite its many applications in industry, it should be noted that CV is one of the cationic synthetic dyes belonging to the triphenylmethane group which easily enters the surface of the cell membrane with a negative charge. This dye is inherently stable in the environment, causing cancer, increased heart rate, hypersensitivity urtication eyes, vomiting, cyanosis, jaundice, and fibrinoid necrosis in humans [10, 15-18]. CV also creates a bright and strong purple color in aqueous solutions that concentration of more than 1.5 mg/lit of it in water causes severe discoloration and as a result can prevent photosynthesis and subsequently reduces oxygen concentration in water [9].

Treatment of industrial effluents contaminated with azo dyes is not easy due to the aromatic and complex structure of these dyes [19]. Today; physical, chemical and biological treatments and sometimes their combination are used to remove these dyes from water [20-22]. Among the most important of these methods are: electrodialysis [23]; chemical oxidation [24]; ozonation [25]; coagulation and flocculation [26]; photocatalytic degradation [27]; ultrafiltration [28]; reverse osmosis [29] and adsorption [30,31].

Among these methods, the adsorption method is widely used for industrial wastewater treatment due to its high speed, simplicity procedure, economic convenience and environmental compatibility [32, 33].

One of the most efficient methods to increase the efficiency of adsorption is the ultrasound based adsorption. Ultrasound waves generate the bubbles within the fluid and increase the porous structure so the efficiency of adsorption increases by raising adsorbent surface area. On the other hand, locally produced high-pressure waves in the fluid increase the mass transfer process among the adsorbent and contaminants [34-37].

In recent years researchers disclosed that organic chemical composites and also hybrid composites based on activated carbons and metal oxides are the best sorbents for azo dyes and industrial contaminants [38-40].

Activated carbons are very popular in the nature and there are several resources for activated

carbons such as eggshells [41], eucalyptus wood [42], bombax cieba [43], date palm and date pits [44], pineapple crown [45], nutshells [46-48], corncob and animal bone [49].

In this study, at first we synthesized ZnS-Ni nanoparticles using microwave assisted coprecipitation method. In second step, we used a new nanocomposite which is composed of the nanoparticles of ZnS-Ni stabilized on activated carbons derived from coconut husk (ZnS-Ni/coco AC) as a cheap adsorbent for elimination of CV from aqueous medium by ultrasound based adsorption method [50,51]. We used a central composite design (CCD) combined with response surface methodology (RSM) according to the desirability function (DF) to study the effects of various parameters such as dye concentration, the amount of adsorbent, sonication time and pH on the process of adsorption and the interaction between various parameters in dye elimination leading to optimum conditions for maximum dye removal from aqueous solutions with the minimum number of experiments [10, 52, 53]. The equilibrium behavior of adsorbent and contaminants and kinetics of the adsorption process is also studied.

MATERIALS AND METHODS

Materials

In this study we used zinc acetate ($Zn(CH_3COO)_2$), thioacetamide (CH_3CSNH_2), nickel sulfate ($NiSO_4$), sodium hydroxide ($NaOH$), hydrochloric acid (HCl), sulfuric acid (H_2SO_4), phosphoric acid (H_3PO_4), sodium chloride ($NaCl$), ethanol, methanol from Merck company and double distilled water from Tehran Kimia-Acid company as raw materials for preparing of our nanomaterials. Crystal Violet (CV) from Merck was selected as dye. The dye chemical structure and its adsorption spectra was illustrated

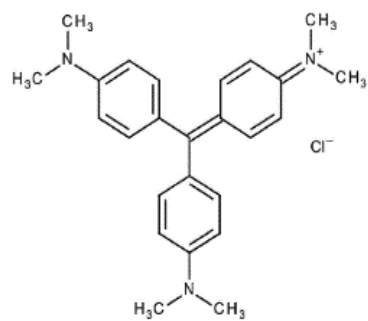


Fig. 1. The chemical structure of Crystal Violet dye.

in Fig. 1.

Devices

Nano particles were synthesized by microwave-assisted co- precipitation using a simple kitchen microwave with power of 180-900Watt from Panasonic company. Morphology of ZnS-Ni nanoparticles was analysed by field emission scanning electron microscopy (FE-SEM: VEGA// TESCAN- LMU). The samples were coated with gold film and acceleration voltage of apparatus was 15.0 kV. The TEM image of ZnS-Ni/coco AC sample was obtained by (TEM: Zeiss-EM10c- 100 kV) microscope. The element composition of samples were analysed by energy- dispersive x-ray spectrometry (EDX). To determine the structural characterization of ZnS:Ni sample, we used XRD analysis with CuK_α radiation ($\lambda=1.5418\text{ \AA}$) operating at 40 kV, 30 mA in the range of $2\theta=10^\circ$ - 80° . Double- beam UV-Vis spectrometer (Hewlett-Packard 8453 diode array controlled by a Hewlett- Packard computer /Agillent) was used to determine the concentrations of dyes in the dye solutions before and after the adsorption. A digital pH meter (M-12//Horiba) was used to measure the pH of solutions. A 40 kHz and 355 W ultrasonic bath was used for assisting the adsorption processes (SONICA 3200ETH S3// SOLTEC, Italy) and the phase separation was carried out using a centrifuge (RST 24S// D.T.A.P, Iran) at 3000 rpm for 5 minutes.

Synthesis of ZnS-Ni nanoparticles

We mixed 16 ml of thioacetamide 0.5 molar

solution with 5 ml of zinc acetate 0.12 molar solution on a magnetic stirrer at a constant temperature of 40 °C to create a white precipitate. Then we add few droplets of concentrated sulfuric acid to dissolve the precipitate. After that 5 ml of nickel sulfate 0.3 molar solution and 24 ml thioacetamide 0.5 molar solution were added. The final volume of the solution was increased to 100 ml and the pH was adjusted to 7.0.

To increase the amount of substance, we repeated this action three times with the same procedure. Then we put the obtained solutions in the microwave with 180 power for 5 minutes to form nanoparticles in solid phase.

Preparation of activated carbon from coconut husk

The method of Mohan et al. [48] was used to prepare activated carbon from coconut shell. Coconut shell after collecting and washing with tap water were dried at room temperature and then placed in phosphoric acid activating solution for 24 hours at a weight ratio of 1:1. After that activated carbon was prepared through slow pyrolysis. Pyrolysis was carried out in an atmosphere controlled furnace under nitrogen (flow rate= $0.1\text{ m}^3\text{h}^{-1}$). The using of nitrogen prevented feed combustion.

The shells were pyrolyzed in a nitrogen-controlled atmosphere (flow rate : $0.1\text{ m}^3\text{h}^{-1}$) in a furnace. The furnace temperature was set on 170°C for 30 minutes and then the temperature increased to 450°C for 1 h. The resulting material was then cooled in ambient temperature and washed several times with double distilled water

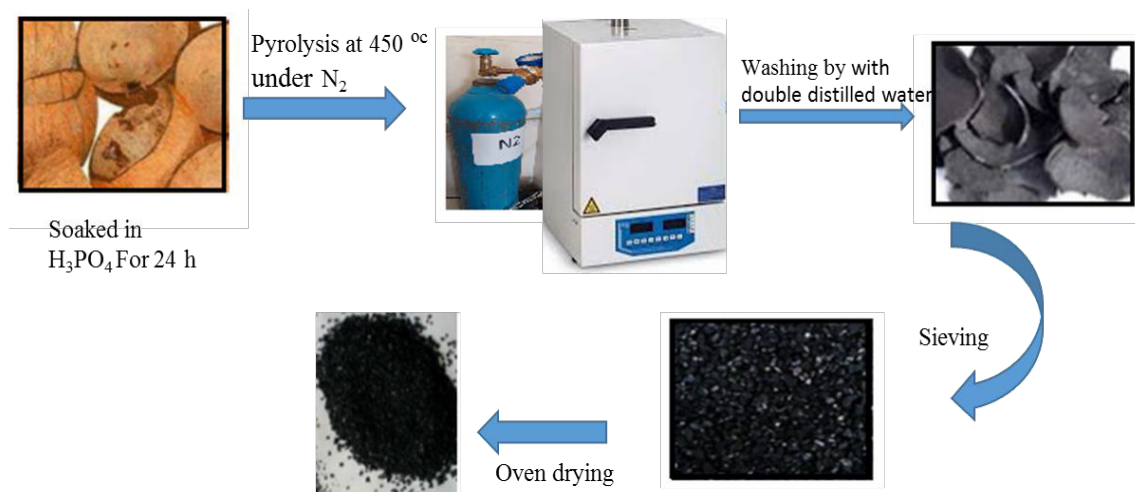


Fig.2. Schematic of activate carbon preparation from coconut shell

to remove any extra contaminants. The washing was continued until pH remained stable at 7.0. Then they were dried for 24 hours at 100 °C and the final product was sieved with 50 µ mesh filter into 50 B.S.S mesh size to obtain uniform and homogeneous particles. Fig. 2 schematically shows the preparation of activated carbon from coconut shell.

Preparation of ZnS-Ni/coco AC

At First, 15 g of activated carbon prepared from coconut husk was poured into 300 ml of double-distilled water and added to the synthesized ZnS-Ni nanoparticles, and the resulting solution was stirred for 20 hours to become uniform. Then it was filtered and washed several times with water and dried in an oven at 60 °C for 15 hours. Schematic of the synthesis of ZnS-Ni nanoparticles and ZnS-Ni/coco AC nanocomposite preparation is shown in Fig. 3.

The resulting material should be used as an adsorbent in dye adsorption experiments.

Ultrasound based adsorption experiment

About 50 ml of CV solutions in different concentrations (5-25 mg/L) where poured to different containers and the pH of the solutions were adjusted between 3 to 8 using 1 M hydrochloric acid and sodium hydroxide.

Then different amounts of the prepared adsorbent (0.003-0.03 g) were added into the colored solutions and the containing including the colored solution plus the adsorbent with different pH were put into the ultrasonic bath and were

sonicated for 2-6 minutes. The contents of various parameters (pH, dye concentration, the amount of adsorbent and sonication time) were considered according to the RSM design.

After going out from ultrasonic bath, the solutions centrifuged and the final absorbance of each at λ_{\max} (594 nm) was determined by UV-Vis spectrometer. All experiments were performed at 3 times and the mean value of the results are reported.

The removal percentage was determined according to the following equation:

$$R\% = \frac{C_0 - C_f}{C_0} \times 100 \quad (1)$$

where C_0 and C_f are the initial and final dye concentrations (mg/L) respectively.

The equilibrium adsorption capacity of ZnS-Ni/coco AC nanocomposite for CV solutions can be expressed by the following equation:

$$q_e = \frac{(C_0 - C_e)V}{W} \quad (2)$$

In the above equation, q_e is the equilibrium adsorption capacity (mg/g), C_0 and C_e are initial and equilibrium concentrations (mg/L) of CV dye, V is the volume (L) of the solution and W is the weight (g) of ZnS-Ni/coco AC nanocomposite sorbent powder.

Central composite design

Central composite design (CCD) was utilized to evaluate the effect of adsorption conditions on the efficiency of CV removal. CCD was performed for four factors (pH (A: 3-8); the amount of adsorbent

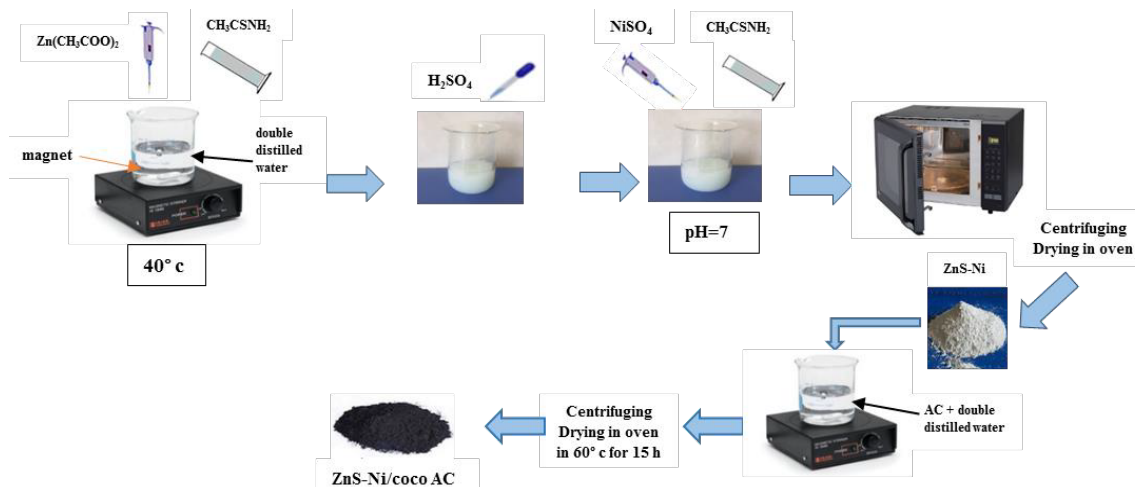


Fig. 3. Schematic of ZnS-Ni nanoparticles and ZnS-Ni/coco AC nanocomposite preparation.

(B: 0.003-0.03 g); dye concentration (C: 5-25 mg/L) and sonication time (D: 2-6 min)) at five levels according to Table 1.

The factor levels were coded as $-\alpha$ (lowest), -1 (low), 0 (middle), 1 (high) and $+\alpha$ (highest). As seen from Table 1, the complete design consisted of 30 runs were done randomly. The model of the

adsorption process is explained by the following quadratic equation:

$$Y = \beta_0 + \sum_{i=1}^k \beta_i X_i + \sum_{i=1}^k \beta_{ii} X_i^2 + \sum_{i=1}^k \sum_{j=1}^{k-1} \beta_{ij} X_i X_j + \varepsilon \quad (3)$$

Table 1. Central Composite Design Parameters Obtained for Various Runs, Experimental Values of four Variables, and Responses for the Adsorption of CV by ZnS-Ni/Coco AC

	Factors		Levels				
			$-\alpha$	Low (-1)	Central (0)	High (+1)	$+\alpha$
Run	pH	Adsorbent mass(g)	CV concentration(mg/L)	Sonication time(min)	Observed	Predicted	R%CV
1	7.00	0.010	16.00	5.00	76.00	76.35	-0.35
2	6.00	0.017	24.00	4.00	88.55	87.99	0.56
3	6.00	0.017	24.00	4.00	89.59	87.99	1.60
4	5.00	0.010	32.00	5.00	74.99	73.46	1.52
5	4.00	0.017	24.00	4.00	78.88	76.25	2.63
6	6.00	0.017	8.00	4.00	95.49	95.08	0.40
7	7.00	0.023	32.00	3.00	70.85	70.90	-0.06
8	6.00	0.017	24.00	6.00	99.88	99.15	0.74
9	7.00	0.023	16.00	3.00	70.32	71.92	-1.60
10	7.00	0.023	32.00	5.00	80.49	80.64	-0.15
11	8.00	0.017	24.00	4.00	52.32	54.26	-1.93
12	7.00	0.010	32.00	3.00	66.79	64.71	2.08
13	5.00	0.010	16.00	3.00	80.46	80.41	0.05
14	6.00	0.017	24.00	4.00	88.21	87.99	0.22
15	5.00	0.010	16.00	5.00	85.99	86.34	-0.35
16	6.00	0.017	24.00	4.00	89.36	87.99	1.38
17	5.00	0.023	32.00	3.00	83.15	83.04	0.10
18	6.00	0.017	24.00	2.00	83.01	83.05	-0.04
19	6.00	0.017	40.00	4.00	81.11	80.82	0.29
20	6.00	0.030	24.00	4.00	84.09	82.22	1.87
21	7.00	0.023	16.00	5.00	94.68	92.75	1.93
22	7.00	0.010	16.00	3.00	62.51	60.96	1.55
23	5.00	0.023	16.00	3.00	89.23	89.60	-0.37
24	6.00	0.003	24.00	4.00	59.37	60.60	-1.23
25	5.00	0.023	16.00	5.00	98.61	100.97	-2.36
26	5.00	0.010	32.00	3.00	76.25	78.62	-2.37
27	6.00	0.017	24.00	4.00	84.07	87.99	-3.91
28	6.00	0.017	24.00	4.00	88.20	87.99	0.22
29	5.00	0.023	32.00	5.00	81.16	83.33	-2.17
30	7.00	0.010	32.00	5.00	68.79	69.01	-0.22

Where Y is the predicted response function (% Removal), β_0 and ε are constant and error terms respectively, X_i and X_j are the coded values of our independent parameters, β_i is the linear coefficient, β_{ii} is the quadratic coefficient and β_{ij} is the interaction coefficient.

The collected number of 30 runs were applied to find mathematical correlate among the independent parameters and the corresponding response values. Results were analyzed by using the analysis of variance (ANOVA) and the validity of the response surface model was investigated by measuring the regression coefficients (R^2) and the lack of fit (LOF) of the model. Moreover, the most effective factors were determined on the basis of F- values and P- values (confidence surface= 0.95). In addition, by plotting the three-

dimensional plots of response (% Removal) vs. significant parameters using Design-Expert 7 software, the best condition of dye adsorption was found graphically [10,54].

RESULTS AND DISCUSSION

Characterization

FESEM and TEM analysis

Fig. 4 shows the images of FESEM analysis of ZnS-Ni nanoparticles. The almost uniform structure of the fine and coarse grains glued to each other with holes between them indicates the passage of the nucleation stage. The porous structure indicates the readiness of a suitable nanostructure of ZnS-Ni for adsorption.

Also FESEM images of activated carbons from coconut husk is seen in Fig. 5. Fine and almost identical grains join to each other to form islands

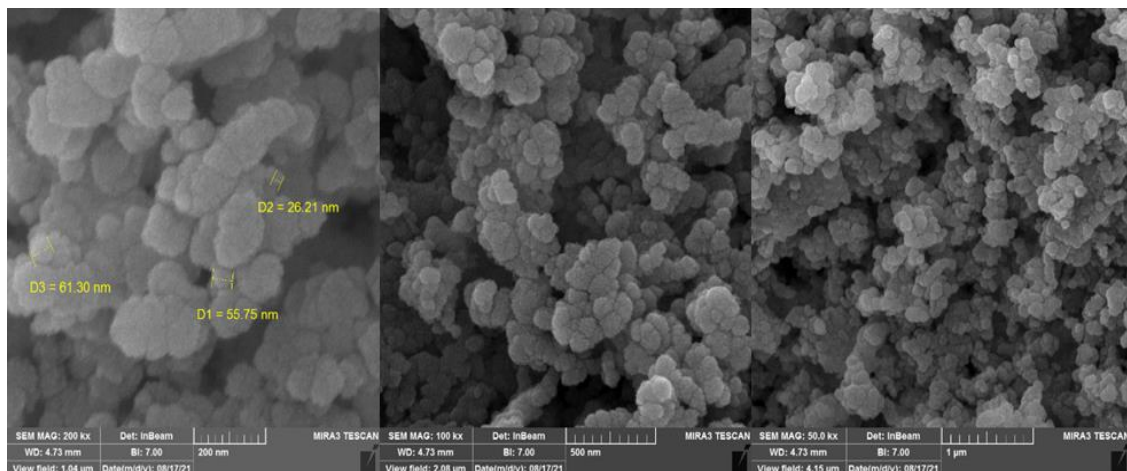


Fig. 4. SEM images of ZnS-Ni nanoparticles.

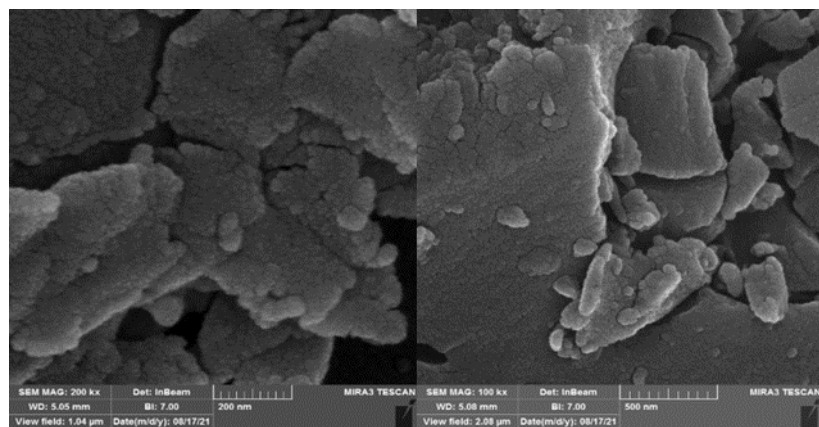


Fig. 5. SEM images of activated carbon.

Table 2. The mean diameter of nanoparticles of ZnS-Ni and activated carbon samples.

Sample	Mean diameter of particles (nm)
ZnS-Ni	49
Activated carbon	61

with voids between them.

FESEM instrument's software revealed that the grain size in both samples were between 30 to 60 nm. The mean diameter of particles of both samples was determined by "motic" measurement software that uses in medical laboratories for determining the size of microscopic components.

Each FESEM image was carried to software medium and 40 particles on it was selected randomly. The boundary of each particle was determined by motic optical pen and the area of it was estimated by software. By considering of each particle as a sphere, the radius of it was calculated. The average of these 40 results was introduced as the mean diameter of particles for each sample. Table 2 indicates the calculated mean diameter of particles in both samples. The mean size less than 100 nm for particles confirms the formation of nanostructure for our samples.

In Fig. 6, TEM images of ZnS-Ni /coco AC was shown. It is evident that the ZnS-Ni nanoparticles are uniformly distributed between nanoparticles of AC. Dark areas revealed more concentration of mass and the light areas reveal foci of less

concentrated mass. So it can be concluded that the nanoparticles of coco AC were surrounded the ZnS-Ni nanoparticles like a shell. The porous and spongy structure of AC not only provides perfect condition for CV adsorption by ZnS-Ni nanoparticles, but also causes more dye to be adsorbed by the activated carbon itself.

The histogram of Fig. 7 shows the particle size in the range of 0 to 50 nm in the prepared nanocomposite which has been drawn from the information obtained from TEM software.

XRD and EDX analysis

Fig. 8 indicates the x-ray diffraction (XRD) patterns of ZnS-Ni sample. In this pattern, there are three large peaks in $2\theta = 29.2^\circ$, 48.8° , 57.8° respectively related to (111), (220) and (311) lattice planes of cubic zinc blend structure according to JCPDS no. 01-080-0020 of ZnS. Largeness of these peaks shows the formation of crystalline phases and high purity of the synthesized sample.

The mean crystallite size of samples was calculated from the full width at half maximum (FWHM) of the diffraction peaks using Debye-

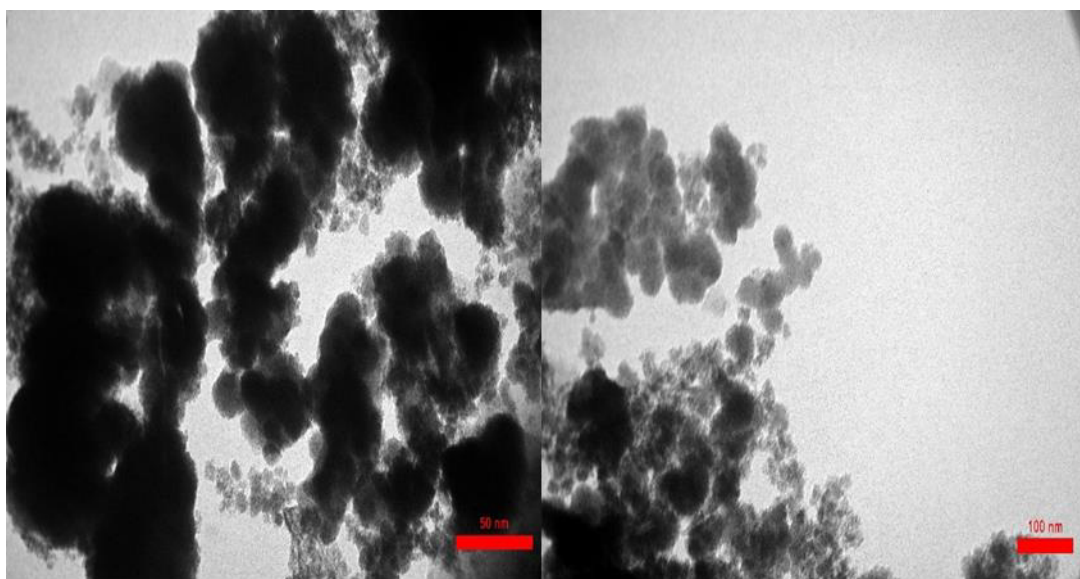


Fig. 6. TEM images of ZnS-Ni/coco AC nanocomposite.

Scherrer's equation:

$$d = \frac{k\lambda}{\beta \cos \theta} \quad (4)$$

where d is the mean crystalline dimension perpendicular to the reflecting phases, λ is the x-ray wavelength, k is Scherrer constant (0.94), β is the FWHM intensity of a Bragg reflection excluding instrumental broadening and θ is the Bragg angle [55]. The calculated mean crystallite size was 5 nm.

Finally, the EDX spectrums of ZnS-Ni nanoparticles and ZnS-Ni/coco AC nanocomposite are seen in Fig. 9a,b. The presence of Zn, S and

Ni peaks indicates the incorporation of these elements in both samples. Sharp and intense peak assign to carbon in Fig. 7b confirms the formation of ZnS-Ni/coco AC nanocomposite.

Experimental Design

RSM approach and statistical analysis

As previously described in this study, CCD method was used to investigate the effect of four factors: pH, sonication time, the amount of sorbent and dye concentration to remove Crystal Violet and determine the necessary conditions for optimizing the results.

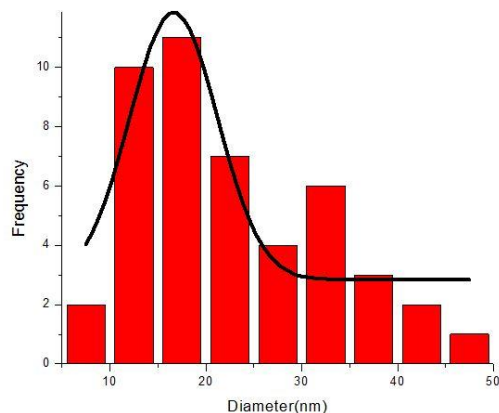


Fig. 7. The histogram of the particle size in the range of 0 to 50 nm in ZnS-Ni/coco AC nanocomposite.

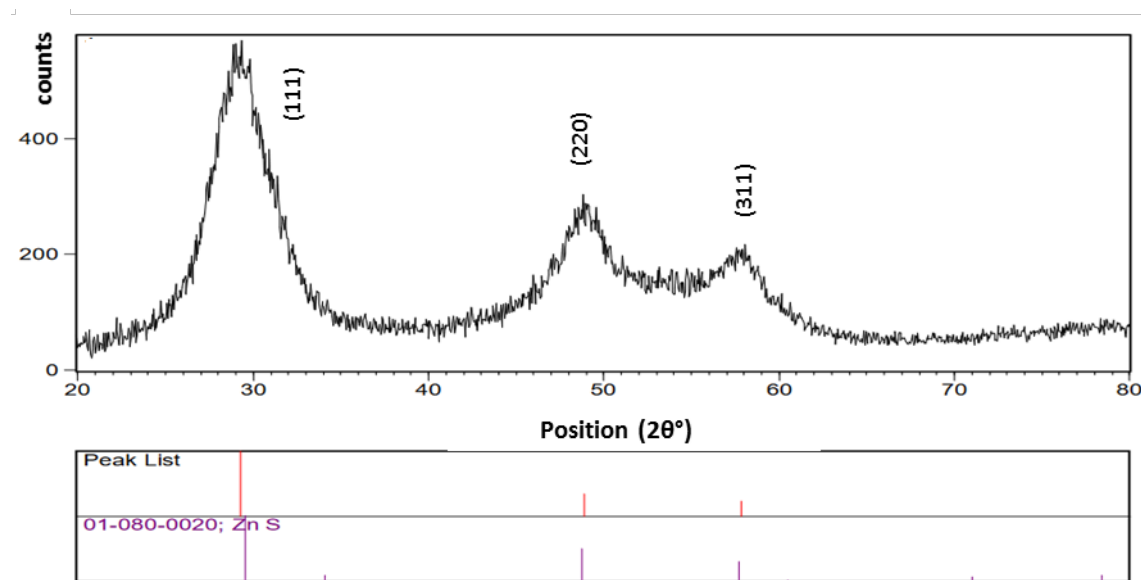


Fig. 8. XRD pattern of ZnS-Ni nanoparticles.

Table 3. Analysis of variance (ANOVA) of the fitted quadratic equations for the adsorption of CV by ZnS-Ni/coco AC.

Source	SS ^a	df ^b	MS ^c	F-value	p-Value	Remark
Model	3707.20	14	264.80	58.13	< 0.0001	significant
A	733.95	1	733.95	161.11	< 0.0001	
B	667.92	1	667.92	146.62	< 0.0001	
C	289.45	1	289.45	63.54	< 0.0001	
D	368.18	1	368.18	80.82	< 0.0001	
AB	3.14	1	3.14	0.69	0.4197	
AC	30.68	1	30.68	6.73	0.0203	
AD	89.46	1	89.46	19.64	0.0005	
BC	22.78	1	22.78	5.00	0.0410	
BD	29.63	1	29.63	6.50	0.0222	
CD	123.00	1	123.00	27.00	0.0001	
A ²	882.42	1	882.42	193.70	< 0.0001	
B ²	437.44	1	437.44	96.02	< 0.0001	
C ²	2.177E-003	1	2.177E-003	4.778E-004	0.9828	
D ²	16.54	1	16.54	3.63	0.0761	
Residual	68.33	15	4.56			
Lack of Fit	48.16	10	4.82	1.19	0.4479	not significant
Pure Error	20.17	5	4.03			
Cor Total	3775.53	29				
Model Summary Statistics						
Model	R ²	R ² Adj	R ² Pred	PRESS	Std. Dev	CV%
Quadratic	0.9819	0.96819	0.91818	307.50	2.13	2.64

^aSum of square, ^bDegree of freedom, ^cMean square

The factors coded in Table 1 are the coefficients and constants calculated through the software and the percentage of color removal (R) is placed in equation 3 and the following equation is obtained:

$$\begin{aligned} \text{R\% CV} = & 87.61 - 5.53A + 5.41B - 3.74C + 3.92D + \\ & 0.46AB + 1.38AC + 2.36AD - 1.24BC + 1.41BD - \\ & 2.77CD - A^2 - 4.05B^2 - 0.008923C^2 + 0.78D^2 \end{aligned} \quad (5)$$

Where A, B, C and D are pH, the amount of adsorbent, dye concentration and sonication time respectively. Parameter analysis and model validity were performed using ANOVA test and the R², LOF, F- value and P- value were determined. Obtained values are demonstrated in Table 3.

The F-value (58.13) indicates the significance of the model [56]. The P-value which is less than 0.0001 means the significance of the parameters [57, 58].

The pH with F-value =141.1 and P< 0.0001 is a powerful factor in dye elimination. For R² and R² adj' the values of 0.9818 and 0.9650 were obtained, respectively, which are close to 1, showing a good correlation between the experimental results and the predicted results. The quadratic equation confirms the value of 98.8% for adsorption. The value obtained for LOF confirms that the predicted values and the actual values correspond to each other. Also, the predicted model has an acceptable

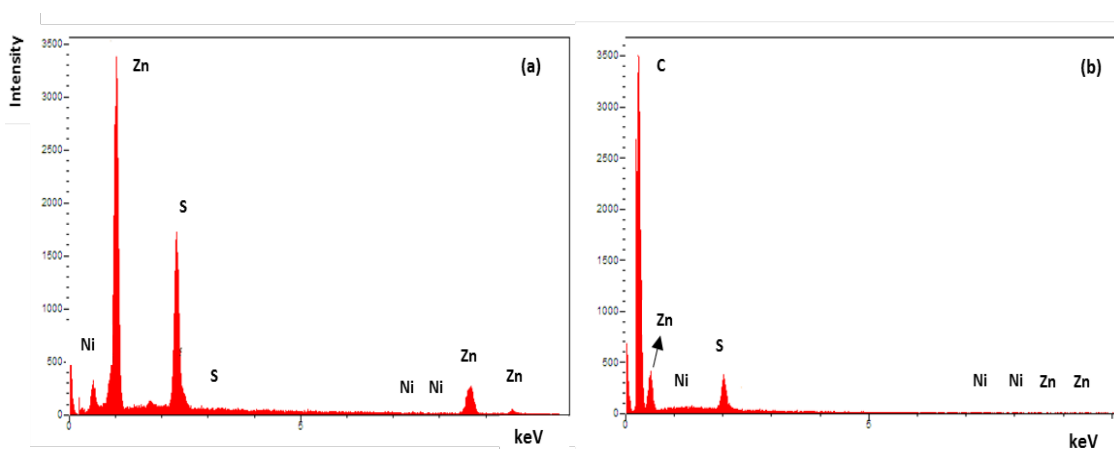


Fig. 9. EDX spectrum of: (a) ZnS-Ni nanoparticles (b) ZnS-Ni/coco AC nanocomposite.

PRESS (Predicted Residual Sum of Square) and adequate precision values of 307.50 and 30.953, respectively, which show the high sensitivity and power of the model and the appropriate signal-to-noise ratio. A value of 2.13 for standard deviation and 2.64 for coefficient of variation also indicates the high accuracy of the model prediction

Adequacy of model

One of the useful tools for determining the adequacy of model is the use of residual charts. The Fig. 10a-d disclose these charts.

In Fig. 10a the normal probability curve is seen. As seen, the residuals are distributed on both sides and very near to line curve and indicates normal distribution and high accuracy of model [59].

In the residual chart in terms of run number (Fig. 10b), random residual values in each run of test is evident because these values do not follow any specific pattern.

Also Fig. 10c disclose the residual values in comparison to predicted values. The presence of residual values on both negative and positive sides reveals the absence of systematic errors in

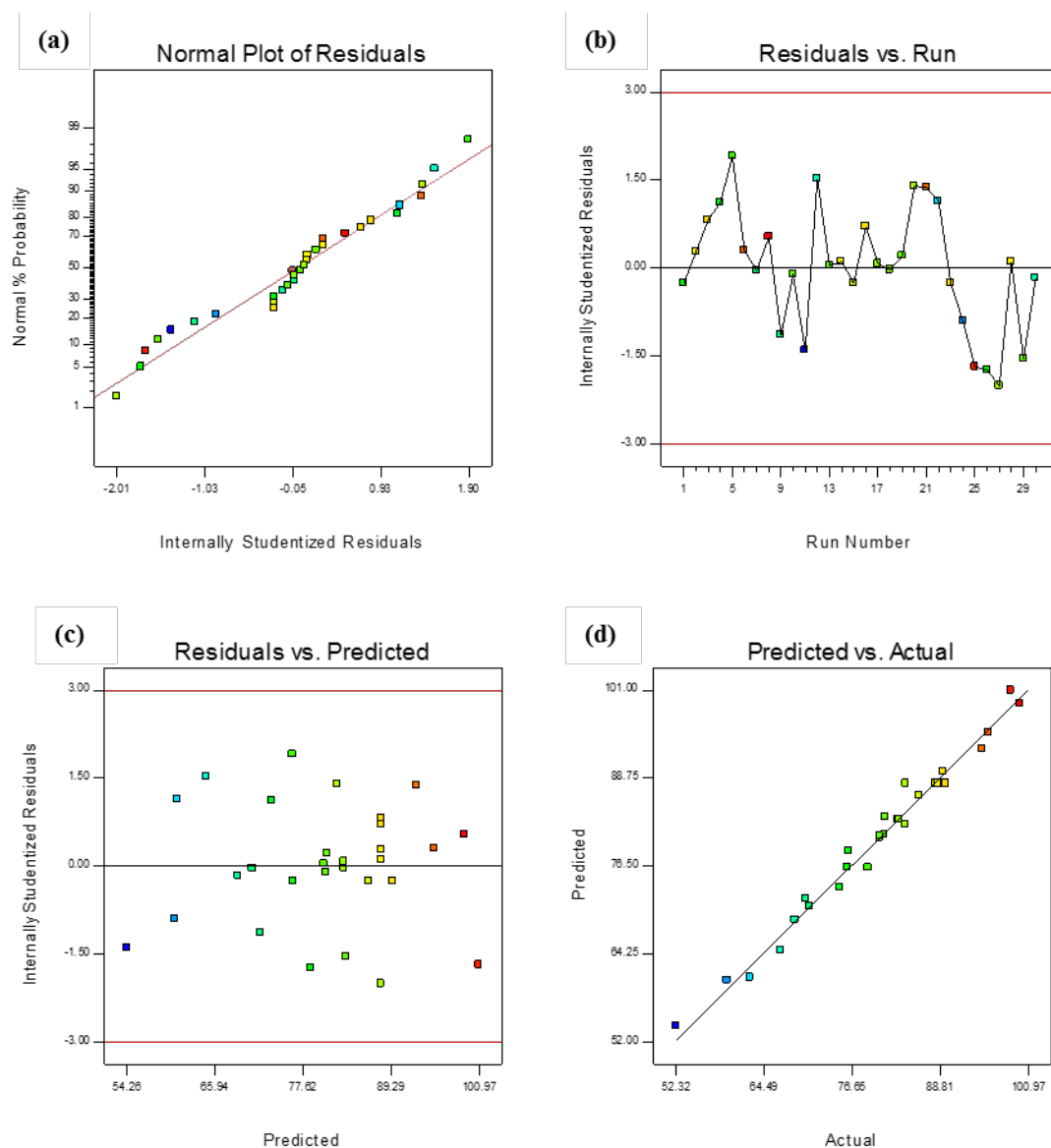


Fig. 10. Observation of efficiency adsorption model of the CV by ZnS-Ni/coco AC by using: (a) normal probability plot (b) residuals versus prediction plot (c) residuals versus run plot and (d) predicted versus actual plot.

performed experiments. In Fig. 10c the random values in each run of test is evident because they're residual values are not consistent with any specific pattern. Finally, Fig. 10d shows the predicted values in terms of the values obtained. All data are close to the line with a slope of 45 degrees, which indicates the normal distribution of data and high

reliability and accuracy of the model. This ensures that this model provides a suitable platform for the process of optimizing the color removal result.

Investigation of the interaction between variables

The Figs. 11a-c show the interaction of color concentration, the amount of adsorbent, pH and

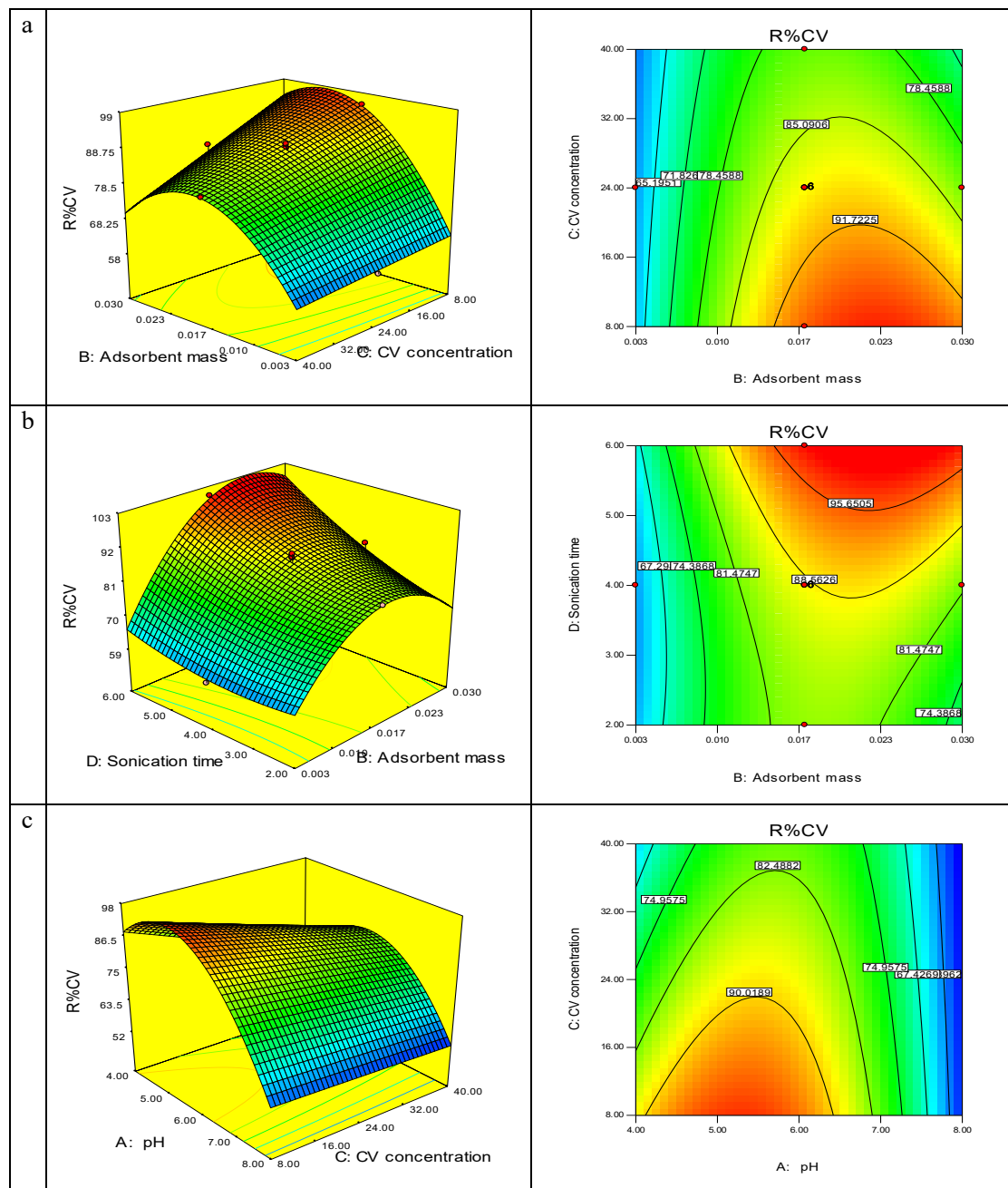


Fig. 11.The 3D response surface and contour plots for the ultrasound assisted adsorption of CV for interactive effect of a) pH and adsorbent dosage, b) Sonication time and CV concentration, c) pH and CV concentration

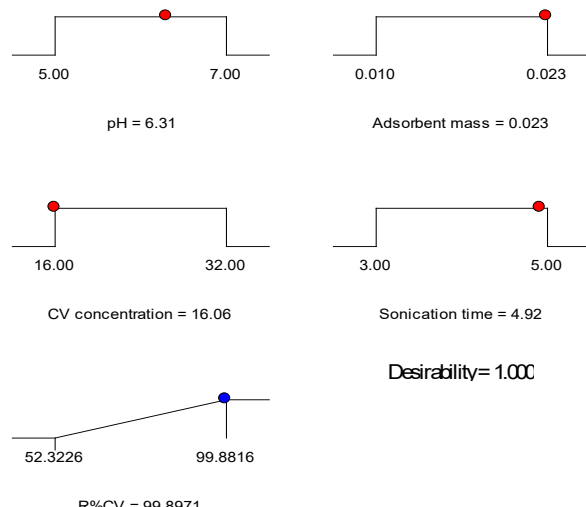


Fig. 12. Optimized process conditions for removing the CV dye.

sonication time on the percentage of CV dye removal which is demonstrated with 3D diagrams and contours.

The diagram 11a shows that lower dye concentration and higher amount of adsorbent lead to higher dye removal percentage. By increasing of the amount of adsorbent, the more active sites are available for the CV dye. If the amount of adsorbent is low, the percentage of dye removal decreases due to insufficient active adsorption sites.

Also, in low concentrations of dye the ratio of dye molecules to active sites will be low, which leads to an increase in the percentage of dye removal.

At high dye concentrations, the active sites of the adsorbent are saturated with dye molecules and the dye removal stops.

But in Fig. 11b, the simultaneous effects of dye concentration and sonication time on the percentage of Crystal Violet removal are examined. As can be seen, at low dye concentration, a shorter time is required for dye adsorption because the number of available active adsorption sites for adsorbing of dye molecules is higher. It

is clear from the figure that the speed of color removal equilibrium is very high, which confirms the efficiency of ultrasound waves to help dye removal. Ultrasound waves causes the adsorbent to be properly dispersed in the solution and the adsorption surface areas to be more available for the dye molecules. Ultrasound also helps to create the porous structures and voids to help the adsorption of more dye molecules.

Finally, Fig. 11c shows that as the pH increases, the percentage of dye adsorption increases. Increasing the pH, increases the reaction sites of the solution and increases the likelihood of electrostatic bonding of the adsorbent with the molecules of cationic CV dye.

At low pH, due to the protonation of the functional groups of ZnS-Ni/coco AC nanoparticles, the surface of adsorbent find positive charge, as a result a strong repulsion occurs between the cationic dye molecules and the positive adsorbent surface, which prevents the accumulation of dye molecules on the adsorbent surface.

Optimization

In the Fig. 12 the optimal conditions for

Table 4. Optimal conditions in experience obtained for removing the color of CV.

Approach	Factors				Removal efficiency (%)	
	pH	Adsorbent mass	CVconcentration	Sonication time	Experimental	predicted
CCD	6.31	0.023	16.06	4.92	98.96±1.03	99.89

removing the CV dye, which has been designed and predicted by the software, can be seen.

In this figure, the effect of different factors on the dye removal response and the optimal values of each factor for dye removal in the ideal state are specified.

Based on the results obtained from the figure, the highest color removal percentage of 99.88% is predicted.

In the Table 4 optimal conditions in experience obtained for removing the color of CV in four repetitions of the experiment is shown which reveal that in the optimal conditions of dye removal, efficacy of about 97.96 % was obtained.

The predicted results were close to the experimental results and disclose that the model designed to remove the color of CV with ZnS-Ni/coco AC nanoparticles is a suitable model.

Adsorption kinetics

The study of the mechanism of the adsorption

process depends on the physical and chemical properties of the system and its conditions.

In this study, two kinetic models (like pseudo first-order and like pseudo second-order) were applied to the adsorption kinetic data under optimal experimental conditions in order to estimate the rate of adsorption mechanism of dye [60]. The fixed parameters and characteristics of each model are listed in Table 5. As shown in Fig. 13a,b the correlation coefficient for like pseudo first and second order models of this absorption is 0.9077 and 0.9994, respectively.

k_1 : Rate constant of pseudo-first order adsorption (min^{-1}), k_2 : second-order rate constant of adsorption ($\text{g mg}^{-1} \text{min}^{-1}$), $q_e(\text{calc})$: equilibrium capacity (mg g^{-1}).

Thus, it is clear that the adsorption process in this study is like pseudo second-order and reveal that the amount of adsorption is highly correlated with the concentration of dye on the adsorbent surface and adsorption occurs in equilibrium.

Table 5. The fixed parameters and characteristics of the kinetic models for the adsorption of CV dye by ZnS-Ni/coco AC.

Model	Equation	Plot	Parameters	Value
Pseudo-first-order	$\ln(q_e - q_t) = \ln(q_e) - k_1 t$	$\ln(q_e - q_t)$ vs. t	$k_1(\text{min}^{-1})$	0.8862
			$q_e(\text{calc})(\text{mg g}^{-1})$	24.1310
			R^2	0.9077
Pseudo-second-order	$\frac{t}{q_t} = \frac{1}{k_2 q_e^2} + \left(\frac{1}{q_e}\right) t$	$\frac{t}{q_t}$ vs. t	$k_2(\text{g mg}^{-1} \text{min}^{-1})$	0.0771
			$q_e(\text{calc})(\text{mg g}^{-1})$	37.7358
			R^2	0.9994
		Experimental data	$q_e(\text{exp})(\text{mg g}^{-1})$	35.8942

k_1 : Rate constant of pseudo-first order adsorption (min^{-1}), k_2 : second-order rate constant of adsorption ($\text{g mg}^{-1} \text{min}^{-1}$), $q_e(\text{calc})$: equilibrium capacity (mg g^{-1}).

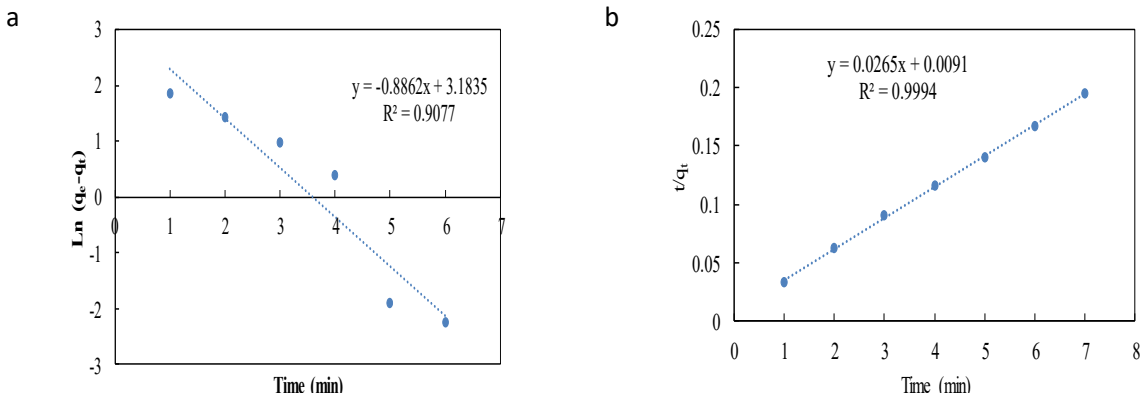


Fig. 13. (a) Pseudo first order kinetics plot (b) Pseudo second order kinetics plot for CV and ZnS-ni/coco AC

Table 6. Constants of the isotherm models calculated for the adsorption of CV by ZnS-Ni/coco AC.

Model	Equation	Plot	Parameters	Value
Langmuir	$\frac{C_e}{q_e} = \frac{1}{K_L q_m} + \frac{C_e}{q_m}$	C_e/q_e vs. C_e	q_m (mg g^{-1})	178.57
	$R_L = \frac{1}{1 + (K_L C_0)}$		K_L (L mg^{-1})	0.2931
			R_L	0.0865
Freundlich	$\ln q_e = \ln K_f + \frac{1}{n} \ln C_e$	$\ln q_e$ vs. $\ln C_e$	R^2	0.9925
			$1/n$	0.8305
			K_f (mg g^{-1}) $(\text{L mg}^{-1})^{1/n}$	32.8581
			R^2	0.988

q_m : maximum adsorption capacity reflected a complete monolayer (mg g^{-1}), K_L : Langmuir constant or adsorption equilibrium constant (L mg^{-1}), R_L indicates the type of isotherm, $1/n$: isotherm constant indicates the empirical parameter, K_f : isotherm constant indicates the capacity parameter (mg g^{-1}) $(\text{L mg}^{-1})^{1/n}$

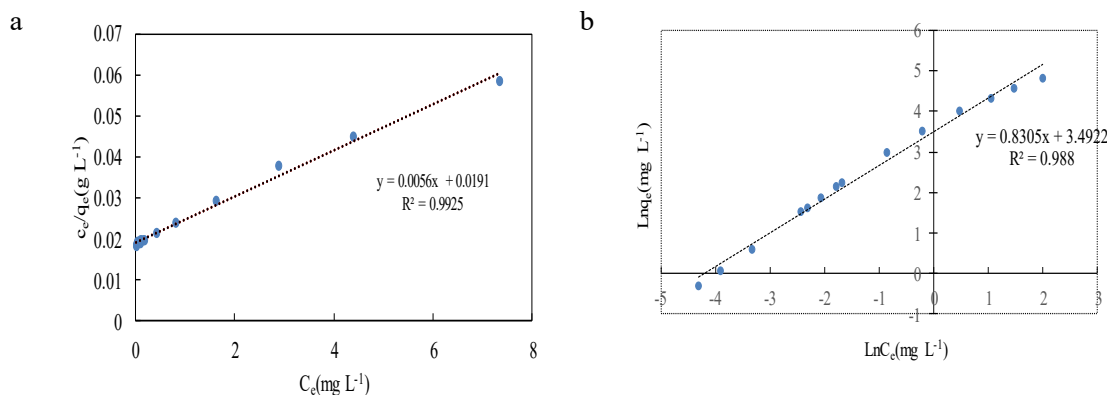


Fig. 14. (a) Langmuir adsorption isotherm (b) Freundlich adsorption isotherm of ZnS-Ni/coco AC nanocomposite.

Table 7. Comparison between the maximum monolayer adsorption of Crystal Violet dye onto the various adsorbents.

Adsorbent	Conditions	Sorption capacity (mg g^{-1})	Ref.
Alg-Cst/Kal	pH = 6.5, T = 35 °C	169.49	62
chitosan aniline composite using peanut waste	pH = 7, room temperature	100.6	63
rice husk		25.46	64
CS/SiO ₂ @ β-CD	pH = 7, T = 30 °C	165	65
Sr _{3.8} Fe _{2.7} O _{7.4} -CMNs	pH = 8, room temperature	33.5	66
activated charcoal	pH = 7.3, room temperature	24	67
ZnS-Ni/Coco AC	pH = 6.3, room temperature	178.57	Present study

On the other hand, close experimental and computational adsorption capacity (q_e) values confirm the following of the like pseudo second-order kinetic model.

Adsorption isotherm

Determination of adsorption isotherm and adsorbent capacity is one of the most important features that should be considered in studies on dye adsorption by different adsorbents [61].

In this study, the number of CV dye molecules

adsorbed on ZnS-Ni /coco AC was described as a function of the initial dye concentration using the Langmuir and Freundlich adsorption isotherms, the results of which are shown in Fig. 14. Also the fixed parameters and characteristics of each adsorption isotherms are listed in Table 6.

Comparison of the results shows that the adsorption capacity is more consistent with the Langmuir adsorption isotherm and the value of the correlation coefficient (R^2) in the Langmuir adsorption isotherm is higher than the value in the

Freundlich adsorption isotherm.

According to Langmuir isotherm, the maximum adsorption capacity (q_e) for dye removal by this adsorbent was estimated to be 178.58 mg/g and the monolayer adsorption process with this isotherm was proposed, which is related to the homogeneous distribution of active sites of ZnS-Ni/coco AC nanoparticles. Also, the Langmuir constant or adsorption equilibrium constant indicates that the desired adsorption value is predicted by this model.

Comparison with other adsorbents

Finally, a comparison between the maximum monolayer adsorption of Crystal Violet dye onto the various adsorbents including our studied nanocomposite is shown in Table 7.

CONCLUSION

In this research, Activated Carbon (AC) was prepared using coconut husk and successfully coated on ZnS-Ni nanoparticles in association with ultrasonic waves to remove Crystal Violet (CV) dye from aqueous solutions. The results obtained from RSM design showed that the factors of dye concentration, the amount of adsorbent, sonication time and pH are effective on the percentage of dye removal and in optimal conditions 99% of dye is removed from the aqueous solution. Using the results obtained from the studies of synthetic parameters, it was concluded that the like pseudo second-order synthetic model is most compatible with the experimental data and the dye removal process on the surface of the adsorbent nanoparticles follows a like pseudo second-order model. This indicates that the speed of the adsorption process is under the control of the dye concentration on the adsorbent surface. Also, dye adsorption isotherm studies on nanoparticle surface followed Langmuir isotherm and the maximum adsorption capacity was 175.57 mg/g with this model.

Thus, it was found that under optimal conditions the use of ZnS-Ni/coco AC adsorbent for elimination of CV dye from aqueous medium by ultrasound based adsorption method has a suitable efficiency.

CONFLICT OF INTEREST

The authors declare that there is no conflict of interests regarding the publication of this manuscript.

REFERENCES

- Hou Y, Chu W, Ma M. Carbonaceous and nitrogenous disinfection by-product formation in the surface and ground water treatment plants using Yellow River as water source. *Journal of Environmental Sciences*. 2012;24(7):1204-1209.
- Ansari MO, Khan MM, Ansari SA, Cho MH. Polythiophene nanocomposites for photodegradation applications: Past, present and future. *Journal of Saudi Chemical Society*. 2015;19(5):494-504.
- Zhang Y, Wu B, Xu H, Liu H, Wang M, He Y, et al. Nanomaterials-enabled water and wastewater treatment. *NanolImpact*. 2016;3-4:22-39.
- Crini G. Non-conventional low-cost adsorbents for dye removal: A review. *Bioresour Technol*. 2006;97(9):1061-1085.
- Chen S, Zhang J, Zhang C, Yue Q, Li Y, Li C. Equilibrium and kinetic studies of methyl orange and methyl violet adsorption on activated carbon derived from Phragmites australis. *Desalination*. 2010;252(1-3):149-156.
- Yagub MT, Sen TK, Afroze S, Ang HM. Dye and its removal from aqueous solution by adsorption: A review. *Advances in Colloid and Interface Science*. 2014;209:172-184.
- Vakili M, Rafatullah M, Ibrahim MH, Abdullah AZ, Salamatinia B, Gholami Z. Chitosan hydrogel beads impregnated with hexadecylamine for improved reactive blue 4 adsorption. *Carbohydr Polym*. 2016;137:139-146.
- Gan T, Sun J, Cao S, Gao F, Zhang Y, Yang Y. One-step electrochemical approach for the preparation of graphene wrapped-phosphotungstic acid hybrid and its application for simultaneous determination of sunset yellow and tartrazine. *Electrochimica Acta*. 2012;74:151-157.
- Oloo CM, Onyari JM, Wanyonyi WC, Wabomba JN, Muinde VM. Adsorptive removal of hazardous crystal violet dye form aqueous solution using Rhizophora mucronata stem-barks: Equilibrium and kinetics studies. *Environmental Chemistry and Ecotoxicology*. 2020;2:64-72.
- Rafiee A, Ghanavati Nasab S, Teimouri A. Synthesis and characterization of pistachio shell/nanodiopsidc nanocomposite and its application for removal of Crystal Violet dye from aqueous solutions using central composite design. *Int J Environ Anal Chem*. 2019;100(14):1624-1649.
- Abdi Z, Maghazei F, Ghanbari D. The Effect of Calcium Perovskite and Newly Developed Magnetic $\text{CaFe}_2\text{O}_4/\text{CaTiO}_3$ Perovskite Nanocomposite on Degradation of Toxic Dyes Under UV-Visible Radiation. *Journal of Cluster Science*. 2021;1-3.
- Masoumi S, Nabiyouni G, Ghanbari D. Photo-degradation of Congored, acid brown and acid violet: photo catalyst and magnetic investigation of $\text{CuFe}_2\text{O}_4-\text{TiO}_2-\text{Ag}$ nanocomposites. *Journal of Materials Science: Materials in Electronics*. 2016;27(10):11017-11033.
- Karbasi M, Maghazei F, Ghanbari D. Magnetic investigation of microwave synthesized and thermal stable poly vinyl alcohol-cobalt ferrite nanocomposites. *Journal of Nanostructures*. 2019;9(2):365-75.
- Tan YN, Wong CL, Mohamed AR. An Overview on the Photocatalytic Activity of Nano-Doped-TiO₂ in the Degradation of Organic Pollutants. *ISRN Materials Science*. 2011;2011:1-18.
- Mohanty K, Naidu JT, Meikap BC, Biswas MN. Removal of Crystal Violet from Wastewater by Activated Carbons Prepared from Rice Husk. *Industrial & Engineering*

- Chemistry Research. 2006;45(14):5165-5171.
16. Au W, Pathak S, Collie CJ, Hsu TC. Cytogenetic toxicity of gentian violet and crystal violet on mammalian cells in vitro. *Mutation Research/Genetic Toxicology*. 1978;58(2-3):269-276.
 17. Saeed A, Sharif M, Iqbal M. Application potential of grapefruit peel as dye sorbent: Kinetics, equilibrium and mechanism of crystal violet adsorption. *J Hazard Mater.* 2010;179(1-3):564-572.
 18. Saha PD, Chakraborty S, Chowdhury S. Batch and continuous (fixed-bed column) biosorption of crystal violet by Artocarpus heterophyllus (jackfruit) leaf powder. *Colloids Surf B Biointerfaces*. 2012;92:262-270.
 19. Roy U, Manna S, Sengupta S, Das P, Datta S, Mukhopadhyay A, et al. Dye Removal Using Microbial Biosorbents. *Environmental Chemistry for a Sustainable World*: Springer International Publishing; 2018. p. 253-280.
 20. Kamran U, Bhatti HN, Iqbal M, Jamil S, Zahid M. Biogenic synthesis, characterization and investigation of photocatalytic and antimicrobial activity of manganese nanoparticles synthesized from Cinnamomum verum bark extract. *J Mol Struct.* 2019;1179:532-539.
 21. Sabzehei M MM, Karimi H, Ghaedi M. Electrospinning preparation of NiO/ZnO composite nanofibers for photodegradation of binary mixture of rhodamine B and methylene blue in aqueous solution: Central composite optimization. *Appl Organomet Chem.* 2018;32(6).
 22. Khataee AR, Dehghan G, Ebadi A, Zarei M, Pourhassan M. Biological treatment of a dye solution by Macroalgae Chara sp.: Effect of operational parameters, intermediates identification and artificial neural network modeling. *Bioresour Technol.* 2010;101(7):2252-2258.
 23. Li X, Jin X, Zhao N, Angelidakis I, Zhang Y. Novel bio-electro-Fenton technology for azo dye wastewater treatment using microbial reverse-electrodialysis electrolysis cell. *Bioresour Technol.* 2017;228:322-329.
 24. Brisset J-L, Benstaali B, Moussa D, Fanmoe J, Njoyim-Tamungang E. Acidity control of plasma-chemical oxidation: applications to dye removal, urban waste abatement and microbial inactivation. *Plasma Sources Sci Technol.* 2011;20(3):034021.
 25. Kanagaraj J, Mandal AB. Combined biodegradation and ozonation for removal of tannins and dyes for the reduction of pollution loads. *Environmental Science and Pollution Research.* 2011;19(1):42-52.
 26. Huang X, Gao B, Yue Q, Zhang Y, Sun S. Compound bioflocculant used as a coagulation aid in synthetic dye wastewater treatment: The effect of solution pH. *Sep Purif Technol.* 2015;154:108-114.
 27. Hamaloğlu KÖ, Sağı E, Tuncel A. Bare, gold and silver nanoparticle decorated, monodisperse-porous titania microbeads for photocatalytic dye degradation in a newly constructed microfluidic, photocatalytic packed-bed reactor. *J Photochem Photobiol A: Chem.* 2017;332:60-65.
 28. Alventosa-deLara E, Barredo-Damas S, Alcaina-Miranda MI, Iborra-Clar MI. Ultrafiltration technology with a ceramic membrane for reactive dye removal: Optimization of membrane performance. *J Hazard Mater.* 2012;209-210:492-500.
 29. Wang J, Zhang T, Mei Y, Pan B. Treatment of reverse-osmosis concentrate of printing and dyeing wastewater by electro-oxidation process with controlled oxidation-reduction potential (ORP). *Chemosphere.* 2018;201:621-626.
 30. Fan L, Luo C, Sun M, Qiu H, Li X. Synthesis of magnetic β -cyclodextrin-chitosan/graphene oxide as nanoabsorbent and its application in dye adsorption and removal. *Colloids Surf B Biointerfaces*. 2013;103:601-607.
 31. Tan P, Hu Y. Improved synthesis of graphene/ β -cyclodextrin composite for highly efficient dye adsorption and removal. *J Mol Liq.* 2017;242:181-189.
 32. Parasuraman D, Serpe MJ. Poly (N-isopropylacrylamide) Micogel-Based Assemblies for Organic Dye Removal from Water. *ACS Applied Materials & Interfaces*. 2011;3(12):4714-4721.
 33. Senthil Kumar P, Varjani SJ, Suganya S. Treatment of dye wastewater using an ultrasonic aided nanoparticle stacked activated carbon: Kinetic and isotherm modelling. *Bioresour Technol.* 2018;250:716-722.
 34. Ashish Chauhan RK. Screening the Effect of Ultrasonic Wave on Effluent Treatment. *Journal of Bioremediation & Biodegradation*. 2015;06(03).
 35. Acisli O, Khataee A, Karaca S, Sheydaei M. Modification of nanosized natural montmorillonite for ultrasound-enhanced adsorption of Acid Red 17. *Ultrason Sonochem.* 2016;31:116-121.
 36. Bazrafshan AA, Ghaedi M, Hajati S, Naghiha R, Asfaram A. Synthesis of ZnO-nanorod-based materials for antibacterial, antifungal activities, DNA cleavage and efficient ultrasound-assisted dyes adsorption. *Ecotoxicology and Environmental Safety*. 2017;142:330-337.
 37. Malekzadeh M, Nejai A, Baneshi MM, Kokhdan EP, Bardania H. The use of starch-modified magnetic Fe⁰ nanoparticles for naphthalene adsorption from water samples: Adsorption isotherm, kinetic and thermodynamic studies. *Appl Organomet Chem.* 2018;32(8):e4434.
 38. Mezohegyi G, van der Zee FP, Font J, Fortuny A, Fabregat A. Towards advanced aqueous dye removal processes: A short review on the versatile role of activated carbon. *J Environ Manage.* 2012;102:148-164.
 39. Zang H, Miao C, Shang J, Liu Y, Liu J. Structural effects on the catalytic activity of carbon-supported magnetite nanocomposites in heterogeneous Fenton-like reactions. *RSC advances.* 2018;8(29):16193-16201.
 40. Streit AFM, Côrtes LN, Druzian SP, Godinho M, Collazzo GC, Perondi D, et al. Development of high quality activated carbon from biological sludge and its application for dyes removal from aqueous solutions. *Sci Total Environ.* 2019;660:277-287.
 41. Girod P, Dufour A, Fierro V, Rogauve Y, Rogauve C, Zoulalian A, et al. Activated carbons prepared from wood particleboard wastes: Characterisation and phenol adsorption capacities. *J Hazard Mater.* 2009;166(1):491-501.
 42. Tancredi N, Medero N, Möller F, Píriz J, Plada C, Cordero T. Phenol adsorption onto powdered and granular activated carbon, prepared from Eucalyptus wood. *Journal of Colloid and Interface Science*. 2004;279(2):357-363.
 43. Bangash FK, Manaf A. Dyes Removal from Aqueous Solution Using Wood Activated Charcoal of Bombax Ceiba Tree. *J Chin Chem Soc.* 2005;52(3):489-494.
 44. Naushad M, Alqadami AA, Al-Kahtani AA, Ahamed T, Awual MR, Tatarchuk T. Adsorption of textile dye using para-aminobenzoic acid modified activated carbon: Kinetic and equilibrium studies. *J Mol Liq.* 2019;296:112075.
 45. Selvanathan N, Subki NS, Sulaiman MA. Dye Adsorbent

- by Activated Carbon. *Journal of Tropical Resources and Sustainable Science (JTRSS)*. 2021;3(1):169-173.
46. Nejadshafee V, Islami MR. Adsorption capacity of heavy metal ions using sulfone-modified magnetic activated carbon as a bio-adsorbent. *Materials Science and Engineering: C*. 2019;101:42-52.
47. Ghaedi M, Mazaheri H, Khodadoust S, Hajati S, Purkait MK. Application of central composite design for simultaneous removal of methylene blue and Pb²⁺ ions by walnut wood activated carbon. *Spectrochimica Acta Part A: Molecular and Biomolecular Spectroscopy*. 2015;135:479-490.
48. Sarswat A, Mohan D. Sustainable development of coconut shell activated carbon (CSAC) & magnetic coconut shell activated carbon (MCSAC) for phenol (2-nitrophenol) removal. *RSC Advances*. 2016;6(88):85390-85410.
49. Adsorption Efficiency of Activated Carbon Produced From Corn Cob for the Removal of Cadmium Ions From Aqueous Solution. *Journal of Environment and Earth Science*. 2019.
50. Karimi R, Yousefi F, Ghaedi M, Dashtian K. Back propagation artificial neural network and central composite design modeling of operational parameter impact for sunset yellow and azur (II) adsorption onto MWCNT and MWCNT-Pd-NPs: Isotherm and kinetic study. *Chemometrics Intelligent Lab Syst*. 2016;159:127-137.
51. Kheirandish S, Ghaedi M, Dashtian K, Heidari F, Pourebrahim F, Wang S. Chitosan extraction from lobster shells and its grafted with functionalized MWCNT for simultaneous removal of Pb²⁺ ions and eriochrome cyanine R dye after their complexation. *Int J Biol Macromol*. 2017;102:181-191.
52. Samarghandi MR, Khiadani M, Foroughi M, Zolghadr Nasab H. Defluoridation of water using activated alumina in presence of natural organic matter via response surface methodology. *Environmental Science and Pollution Research*. 2015;23(1):887-897.
53. Karimifard S, Alavi Moghaddam MR. Application of response surface methodology in physicochemical removal of dyes from wastewater: A critical review. *Sci Total Environ*. 2018;640-641:772-797.
54. Dastkhoon M, Ghaedi M, Asfaram A, Alipanahpour Dil E. Comparative study of ability of sonochemistry combined ZnS:Ni nanoparticles-loaded activated carbon in reductive of organic pollutants from environmental water samples. *Polyhedron*. 2020;180:114341.
55. Edwards AJ, H.P. Klug and L.E. Alexander, x-ray diffraction procedures for polycrystalline and amorphous materials. *Anal Chim Acta*. 1975;77:349.
56. Kamari S, Ghorbani F, Sanati AM. Adsorptive removal of lead from aqueous solutions by amine-functionalized magMCM-41 as a low-cost nanocomposite prepared from rice husk: Modeling and optimization by response surface methodology. *Sustainable Chemistry and Pharmacy*. 2019;13:100153.
57. Stoica-Guzun A, Stroescu M, Jinga SI, Mihalache N, Botez A, Matei C, et al. Box-Behnken experimental design for chromium(VI) ions removal by bacterial cellulose-magnetite composites. *Int J Biol Macromol*. 2016;91:1062-1072.
58. Lai Y, Annadurai G, Huang F, Lee J. Biosorption of Zn(II) on the different Ca-alginate beads from aqueous solution. *Bioresour Technol*. 2008;99(14):6480-6487.
59. Dil EA, Ghaedi M, Ghezelbash GR, Asfaram A. Multi-responses optimization of simultaneous biosorption of cationic dyes by live yeast *Yarrowia lipolytica* 70562 from binary solution: Application of first order derivative spectrophotometry. *Ecotoxicology and Environmental Safety*. 2017;139:158-164.
60. Maghazei F, Ghanbari D. The Study of Nanostructure, Magnetic Properties and Photocatalytic Behavior of Fe₃O₄/Ag Nanocomposites Synthesized by Microwave Method. *Advanced Materials and New Coatings*. 2020;9(34):2462-73.
61. Sarojini G, Venkatesh Babu S, Rajamohan N, Rajasimman M. Performance evaluation of polymer-marine biomass based bionanocomposite for the adsorptive removal of malachite green from synthetic wastewater. *Environ Res*. 2022;204:112132.
62. Mittal J, Ahmad R, Ejaz MO, Mariyam A, Mittal A. A novel, eco-friendly bio-nanocomposite (Alg-Cst/Kal) for the adsorptive removal of crystal violet dye from its aqueous solutions. *International Journal of Phytoremediation*. 2021;24(8):796-807.
63. Tahir N, Bhatti HN, Iqbal M, Noreen S. Biopolymers composites with peanut hull waste biomass and application for Crystal Violet adsorption. *Int J Biol Macromol*. 2017;94:210-220.
64. Quansah JO, Hlaing T, Lyonga FN, Kyi PP, Hong S-H, Lee C-G, et al. Nascent Rice Husk as an Adsorbent for Removing Cationic Dyes from Textile Wastewater. *Applied Sciences*. 2020;10(10):3437.
65. Tian T, Liu M, Li Y, Han J, Ren L, Lorenz H, et al. β-Cyclodextrin carbon-based nanoparticles with a core-shell-shell structure for efficient adsorption of crystal violet and bisphenol A. *Particuology*. 2022;62:88-97.
66. Ge Y-M, Zhao X-F, Xu J-H, Liu J-Z, Yang J-S, Li S-J. Recyclable magnetic chitosan microspheres with good ability of removing cationic dyes from aqueous solutions. *Int J Biol Macromol*. 2021;167:1020-1029.
67. Hassan MR, Yakout SM, Abdeltawab AA, Aly MI. Ultrasound facilitates and improves removal of triphenylmethane (crystal violet) dye from aqueous solution by activated charcoal: A kinetic study. *Journal of Saudi Chemical Society*. 2021;25(6):101231.